European Journal of Pharmaceutics and Biopharmaceutics 142 (2019) 165–178

Contents lists available at ScienceDirect

European Journal of Pharmaceutics and Biopharmaceutics

journal homepage: www.elsevier.com/locate/ejpb

Research paper

Stability behaviour of antiretroviral drugs and their combinations. 10: LC-HRMS, LC-MS^n, LC-NMR and NMR characterization of fosamprenavir degradation products and in silico determination of their ADMET properties

Dilip Kumar Singh[a], Archana Sahu[a], Aabid Abdullah Wani[b], Prasad V. Bharatam[b], Chinmaya Narayana Kotimoole[c], Kedar Balaji Batkulwar[c], Abhijeet Yashwantrao Deshpande[c], Sanjeev Giri[c], Saranjit Singh[a,*]

[a] Department of Pharmaceutical Analysis, National Institute of Pharmaceutical Education and Research (NIPER), Sector 67, S.A.S. Nagar 160 062, Punjab, India
[b] Department of Medicinal Chemistry, National Institute of Pharmaceutical Education and Research (NIPER), Sector 67, S.A.S. Nagar 160 062, Punjab, India
[c] DMPK and Pharmaceutical Development, Aurigene Discovery Technologies Limited, Hyderabad 500 049, Telangana, India

ARTICLE INFO

Keywords:
Fosamprenavir
Forced degradation
Degradation products
LC-MS
LC-NMR
NMR
ADMET Predictor™

ABSTRACT

The present study focused upon the forced degradation behaviour of fosamprenavir (FPV), an antiretroviral drug. A total of six degradation products (DPs) were separated on a non-polar stationary phase by high performance liquid chromatography (HPLC). For the characterization, comprehensive mass fragmentation pathway of the drug was initially established using high resolution mass spectrometry (HRMS) and multi-stage tandem mass spectrometry (MS^n) data. Subsequently, LC-HRMS and LC-MS^n studies were carried out on the forced degraded samples containing the DPs. Five DPs were isolated and subjected to extensive 1D (^{1}H, ^{13}C, and DEPT-135 (distortionless enhancement by polarization)) and 2D (COSY (correlation spectroscopy), TOCSY (total correlation spectroscopy), HSQC (heteronuclear single quantum coherence) and HMBC (heteronuclear multiple bond correlation)) nuclear magnetic resonance (NMR) studies to ascertain their structures, while one degradation product was subjected to LC-NMR studies, as it could not be isolated. The collated information was helpful in characterization of all the DPs, and to delineate the degradation pathway of the drug. Additionally, physicochemical, as well as absorption, distribution, metabolism, excretion and toxicity (ADMET) properties of the drug and its DPs were evaluated in silico by ADMET Predictor™ software.

1. Introduction

Forced degradation (stress testing) is an important part of the drug development process. These studies help in (i) facilitation of the development of stability-indicating analytical methodology, (ii) gaining understanding of intrinsic stability of the drug substance, and (iii) laying down the degradation pathway [1]. For the latter, it is important to characterize the major and minor degradation products (DPs) unequivocally, which is increasingly being done by employing hyphenated instrumental techniques (LC-MS, LC-NMR, etc.) [2–10].

The present study involved investigation of degradation behaviour of fosamprenavir calcium (FPV), which is chemically calcium (2R,3S)-1-(4-amino-N-isobutylphenylsulfonamido)-4-phenyl-3-(((S)-tetrahydrofuran-3-yloxy)carbonylamino)butan-2-yl phosphate. It is an oral prodrug of amprenavir, which is a protease inhibitor (PI) of human immunodeficiency virus type 1 (HIV-1). The drug rapidly hydrolyzes *in vivo* to form amprenavir (active moiety) by cellular phosphatases [11,12]. Due to slow kinetic wetting profile and high lipophilicity of amprenavir, a phosphate ester prodrug of amprenavir was developed, to help in reduction of pill burden and improvement in patient compliance [13,14]. The formulated product of FPV is marketed under trade names Lexiva™ in the United States (US) and as Telzir® in Europe. Literature review reveals absence of comprehensive and systematic report on degradation behaviour of FPV, although a few reports exist on the development of its stability-indicating method [15–17].

This communication, which is in a series of our publications on stability behaviour of antiretroviral drugs and their combinations [18–26], systematically and comprehensively explores comprehensive degradation behaviour of FPV and also reports the predicted physicochemical and ADMET properties of the drug and its identified DPs.

* Corresponding author.
E-mail address: ssingh@niper.ac.in (S. Singh).

https://doi.org/10.1016/j.ejpb.2019.06.018
Received 30 April 2019; Received in revised form 11 June 2019; Accepted 17 June 2019
Available online 19 June 2019
0939-6411/ © 2019 Elsevier B.V. All rights reserved.

2. Experimental

2.1. Drug and reagents

Pure fosamprenavir calcium was obtained as gratis sample from Hetero Drug Ltd. (Hyderabad, India). Hydrochloric acid (HCl), sodium hydroxide (NaOH), hydrogen peroxide (H_2O_2) and buffer salts were of analytical grade and purchased from local manufacturers. Both methanol (CH_3OH) and acetonitrile (CH_3CN) were HPLC grade and were sourced from J.T. Baker, Phillipsburg, NJ, USA. Deuterated dimethyl sulfoxide (DMSO-d_6), deuterated water (D_2O) and NMR grade acetonitrile were purchased from Sigma-Aldrich, St. Louis, Missouri, USA. Ultra-pure water was generated in house using a bench-top purification system (ELGA, High Wycombe, UK).

2.2. Apparatus and equipments

An oil bath (Jain Scientific Glass Works, Ambala, Haryana, India) was used for the degradation studies in the solution state. All solid state thermal forced degradation studies were conducted using a Dri-Bath (Thermolyne, Dubuque, IA, USA). Photostability studies were carried out in a chamber (KBWF 240, WTC Binder, Tuttlingen, Germany) equipped with light bank on the inside top. The latter consisted of a combination of three UV (OSRAM L18 W/73) and three white fluorescent (Philips, Trulite) lamps, in accordance with Option 2 described in ICH guideline Q1B [27]. Visible illumination and near UV energy were measured using a lux meter (model ELM 201, Escorp, New Delhi, India) and near UV-A radiometer (model 206, PRC Krochmann GmbH, Berlin, Germany), respectively. pH/Ion analyzer used to check the pH was model MA 235 from Mettler Toledo, Schwerzenbach, Switzerland. It was calibrated using buffer tablets (Fischer Scientific, Mumbai, India). Sonicator (PowerSonic 510, Hwashin Technologies, Seoul, Korea), precision analytical balance (TB-215D, Denver Instruments, Germany) and autopipettes (Eppendorf, Hamburg, Germany) were the other small equipment employed.

A LC-2010C HT liquid chromatograph (Shimadzu, Kyoto, Japan) was used for separation of drug and its DPs. The same was equipped with a diode array detector (SPD-M20A prominence from Shimadzu) and Inertsil phenyl column (250 × 4.6 mm, 5 μm) (LCGC Chromatography Solutions, Hyderabad, India).

High resolution accurate mass analysis was carried out by using Thermo Scientific™ Q Exactive Plus™ Orbitrap MS (Thermo Fisher Scientific, Bremen, Germany) interfaced to a Thermo Scientific Dionex UltiMate™ 3000 UHPLC system (Thermo Fisher Scientific, San Jose, CA, USA), which was equipped with Acquity UPLC HSS T3 column (100 × 2.1 mm, 1.8 μm) from Waters Corporation, Milford, MA, USA. The ionization was carried out by heated electrospray interface (HESI) in a positive electrospray ionization (+ESI) mode. Instrument control and data processing were carried out using Xcalibur™ version 4.0 QF2. The Q Exactive Plus™ Orbitrap MS was calibrated daily with a mixture of n-butylamine (0.0005%), caffeine (20 μg), MRFA (Met-Arg-Phe-Ala) (10 μg) and ultramark® 1621 (0.001%) in 10 mL solution of acetonitrile:methanol:water:acetic acid (50:25:24:1).

A LC-MS ion trap instrument (Thermo, San Jose, USA) was employed for multi-stage mass (MS^n) experiments. It was equipped with Accela LC that was connected to LTQ-XL-MS 2.5.0. Data acquisition and processing were done using Xcalibur™ (Version 2.0.7SP1) software.

JNM-ECA 500 MHz spectrometer (JEOL, Tokyo, Japan) coupled to prominence HPLC system (Shimadzu, Kyoto, Japan) was used for generation of LC-NMR data. These were controlled by Delta (Version 4.3.5) and LC-NMR Dio (Version 2.0) software, respectively. NMR studies were performed on the same system after detaching the LC probe. In both cases, the data were processed post acquisition by Delta (Version 5.3) software.

2.3. Forced degradation studies

Forced degradation studies were carried out under hydrolytic, oxidative, photolytic and thermal conditions according to the previously described protocol from our laboratories [28,29]. Drug stock solution (2 mg/mL) was prepared in CH_3OH:H_2O (50:50 v/v). Acidic and alkaline hydrolyses were carried out in different molar concentrations of HCl and NaOH, while neutral hydrolysis was performed in CH_3OH:H_2O (50:50 v/v). The temperature of hydrolytic reactions was 75 °C. Final drug concentration in all the stressed solutions was 1 mg/mL. Oxidative forced degradation study was carried out in 3% H_2O_2 at RT. Photolytic studies were carried out by exposing the solid drug in a form of a thin layer. Also, drug solutions prepared in 0.1 N HCl, 0.1 N NaOH and CH_3OH:H_2O (50:50 v/v) were exposed to ICH prescribed dose of light [27]. Dark controls were kept parallelly for comparison. Thermal forced degradation was carried out by sealing the drug in a glass ampoule, and heating the same in a thermostatic block at 60 °C for 21 days.

2.4. Sample preparation for HPLC analysis

Acidic and basic stressed samples were withdrawn at suitable time intervals and neutralized by adding opposite solution of acid or base, while rest of the samples were also withdrawn at suitable time intervals and diluted with CH_3OH:H_2O (50:50 v/v) to a drug concentration of 0.5 mg/mL before injecting into HPLC.

2.5. Liquid chromatographic method development and optimization

An acceptable separation of the drug and its DPs was achieved on the LC column by optimizing the mobile phase components and their proportions, buffer concentration, pH, flow rate and column temperature. A desirable separation and resolution was obtained using a mobile phase composed of methanol and 10 mM ammonium formate buffer (pH 4.0), which was run in a gradient mode (Table S1) at a flow rate of 1 mL/min. The detection wavelength and injection volume were 265 nm and 10 μL, respectively. The column temperature was ambient. The details of LC conditions and optimized methods for semi-preparative HPLC, $LC\text{-}MS^n$, LC-HRMS and LC-NMR studies are given in Table S1.

2.6. Enrichment and isolation of degradation products

For isolation of DPs, higher concentration drug solutions (150 mg/mL) were prepared in CH_3OH:H_2O (50:50 v/v), which were mixed with equal volume of 2 N HCl and 2 N NaOH. These reaction solutions were heated at 75 °C for the period resulting in sufficient conversion of drug to DPs. The DPs were separated on a semi-preparative column (Table S1). In each case, the purity of collected fractions was established by employing analytical HPLC method given in Table S1. The fractions were mixed and dried on a rotary evaporator and the residue was subjected to extensive NMR studies. Of the six DPs, isolation of DP 3 could not be done in pure form, so this particular DP was characterized by using LC-NMR data.

2.7. MS studies (HRMS, MS^n, LC-HRMS and $LC\text{-}MS^n$) on the drug and its degradation products

For comprehensive information on fragmentation pathway of the drug, HRMS and MS^n studies were performed in ESI positive mode by using Orbitrap and ion trap (LTQ-XL) mass spectrometers, respectively. A 5 ppm solution (CH_3OH:H_2O (50:50 v/v)) of FPV was used for both the studies, which were carried out by direct infusion of the drug solution into the respective mass spectrometer at a flow rate of 10 μL/min. The HRMS and MS^n instrument parameters were duly optimized to obtain good intensity of molecular and fragment ions (Tables S2 and

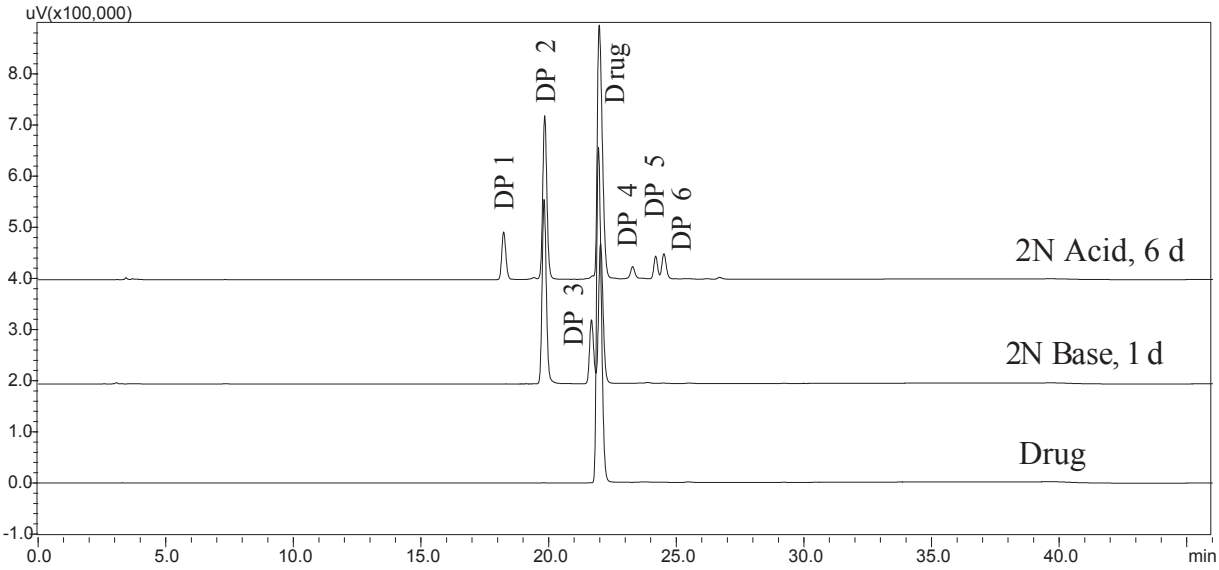

Fig. 1. Chromatograms showing seperation of six degradation products (DPs 1–6) of fosamprenavir (FPV).

S3). For the characterization of DPs, LC-HRMS studies were carried out on isolated fractions of each DP (see Table S1 for LC method details). The accurate masses of protonated molecule and fragment ions of each DP were recorded using parameters optimized for the drug (Table S2). Additionally, LC-MS^n studies were carried out on the stressed samples to establish fragmentation pathway of each DP. In this case, LC method used was similar to the one employed for the analyses of the stressed samples (see Table S1). However, the solvent flow into the MS source was reduced by 1/3 using a divert valve.

2.8. NMR studies on the drug and its degradation products

Separate solutions of the drug and its isolated DPs were prepared in DMSO-d_6. Subsequently, 1D (^{1}H, ^{13}C and DEPT-135) and 2D (COSY, TOCSY, HSQC and HMBC) NMR spectra were acquired using a PFG 5 mm BBO probe at 298 K. ^{1}H NMR spectra were acquired with a ~16 kHz sweep width using 32 K time-domain points with an acquisition time of 3.49 s. ^{1}H NMR spectra of DPs were recorded using the double presaturation pulse sequence for the suppression of moisture and residual solvent signals. D_2O was used for hydrogen/deuterium (H/D) exchange studies. ^{13}C NMR spectra were recorded at 125 MHz with decoupling or off-resonance partial proton decoupling: spectral width 39 kHz, 32 K data points with digital resolution of 1.19 Hz. All one dimensional spectra were processed with an exponential function of 0.2 Hz and a zero filling factor of 1. ^{1}H NMR chemical shifts values were referenced to tetramethylsilane (δ 0.00 ppm) present in DMSO-d_6 solvent, whereas those of ^{13}C NMR were referenced to DMSO-d_6 (δ 39.50 ppm). The 2D COSY and TOCSY spectra were acquired using a total of 8 and 12 scans, respectively. The 2D HSQC and HMBC spectra were acquired with total scans of 3072 (12 * 256 increments) and 9216 (36 * 256 increments), respectively. The 2D NMR spectra were processed using sine bell function.

2.9. LC-NMR studies on the drug and degradation product 3 (DP 3)

As DP 3 was difficult to isolate, in this specific case, the stressed sample was subjected to LC-NMR analysis for recording of ^{1}H NMR spectra. The details of LC conditions and optimized isocratic method are given in Table S1. The peaks were collected in the fraction loop using a terminal cube and sent to inverse 3 mm flow probe, equipped with ^{1}H {13C} channels and pulsed-field gradient along the z-axis. The active sample volume of the probe was approximately 60 μL and transfer time from UV cell to active volume was 42 s at a flow rate of 0.5 mL/min. One-dimensional LC-^{1}H NMR spectra were recorded using WET pulse sequences, with 63 [dB] attenuated power to suppress the solvent signals (CH_3CN and HOD), which gave digital resolution of 0.76 Hz per point. The spectra were acquired with 12.52 kHz spectral width and 16 K data points with 1.30 s of acquisition time for each scan. The chemical shifts were referenced to the methyl signal of residual CH_3CN at δ 1.93 ppm. 2D COSY spectrum was acquired for only the drug using WET pulse sequences for solvent suppression. Acquisition of LC-COSY spectrum of DP 3 was not successful due to its low concentration.

2.10. Quantum chemical analysis

GAUSSIAN09 suite of programmes [30] was used for the quantum chemical analysis. Full geometry optimizations were performed on various conformers of FPV and DP 5 by applying density functional theory (DFT) using B3LYP method [31,32]. The basis set used was 6-31 + G(d). Frequency calculations were carried out on all the structures to verify stationary point with zero negative frequency. ^{1}H NMR chemical shifts of the drug and different conformers of DP 5 were estimated using the Gauge-Independent Atomic Orbitals (GIAO) method [33,34], which is widely used for the calculation of magnetic properties (e.g., shielding/deshileding constants, anisotropies, etc.) of chemical systems [35].

2.11. In silico prediction of physicochemical, as well as absorption, distribution, metabolism, excretion and toxicity (ADMET) properties of the drug and its degradation products

ADMET Predictor™ software (version 9.0.0.10, Simulation Plus, Lancaster, CA, USA) was employed for the prediction of physicochemical, and absorption, distribution, metabolism, excretion and toxicity (ADMET) properties [36] of the drug and its six DPs.

3. Results and discussion

3.1. HPLC chromatograms of the stressed samples and drug degradation behaviour

Typical chromatograms depicting separation of the drug and the DPs are shown in Fig. 1. A total of six DPs were formed under acidic and basic solution stress conditions. Acidic stress (2 N HCl, 75 °C, 6 days)

Table 1
MS^n data of fosamprenavir (FPV).

MS^n	Precursor ion (m/z)	Product ion(s) (m/z)
MS^2	586	498, 488, 431, 429, 418
MS^3	498	400, 357, 344, 301, 255, 245, 243, 241, 229, 202, 200, 189, 156
	488	418, 400, 374, 357, 261, 255, 245, 241, 234, 200, 190, 189, 156
	431	413, 343, 325, 299
	429	411, 341, 323, 297
MS^4	418	400, 374, 362, 357, 318, 263, 261, 255, 253, 245, 241, 229, 219, 217, 202, 200, 189, 172, 156, 146, 129, 120
	413	343, 325, 299
	411	341, 323, 297
	234	190*
MS^5	400	357, 344, 336*, 301, 255, 245, 243, 241, 229, 202, 189, 172, 156, 146, 129
	374	357, 318, 301, 293, 255, 253, 241, 225, 219, 217, 202, 200, 173, 156, 146, 144, 129, 120, 108
	362	318, 301, 225, 156, 146, 129, 108
	343	325*, 299*
	341	323*, 299*
	263	245, 219, 202, 146, 129, 120
	261	243, 217, 200, 144, 120
MS^6	357	301, 293*, 253*, 255, 241, 202, 200, 156
	344	301
	318	301, 225, 173, 156, 146, 129, 108
	245	202, 189, 172, 146, 129
	243	200, 144
	219	202, 120
	217	200, 120
MS^7	301	225*, 173*, 156, 146
	255	241, 229, 156, 108
	202	146, 129
	200	144*
	189	172, 146, 129
MS^8	241	156
	229	156
	172	129
	146	129
MS^9	156	108

* Ions were not captured for further MS^n studies.

resulted in the formation of five DPs (DPs 1–2 and 4–6), while only two (DPs 2 and 3) were generated in the basic (2 N NaOH, 75 °C, 1 day) environment, with DP 2 being common in both the conditions. The drug did not show any degradation upon oxidative, photolytic and thermal stress.

Under acid stress condition indicated above, the drug decomposed upto 45.79%, resulting in 7.70% of DP 1, 28.80% of DP 2, 1.69% of DP 4, 3.53% of DP 5 and 4.07% of DP 6. Similarly, 62.39% drug was degraded in basic stress condition forming DPs 2 and 3 to an extent of 46.49% and 15.90%, respectively. All these % values are on area normalization basis.

3.2. MS studies on the drug

The HRMS mass spectrum of the drug is shown in Fig. S1. The corresponding MS^n data are listed in Table 1. The experimental HRMS data were subjected to elemental composition calculator to obtain most probable molecular formulae, error (in mmu), ring plus double bonds (RDB) and losses for each fragment. The compiled data are listed in Table 2. The information in Tables 1 and 2 were taken into account to establish the fragmentation pathway of the drug, which is outlined in Fig. 2. As depicted, the protonated molecule (FPV, m/z 586) got fragmented in MS^2 step via four different pathways, independently involving neutral loss of $C_6H_7NO_2S$, $C_6H_5NO_2S$, $C_4H_8O_2$ and H_3PO_4 resulting in product ions of m/z 429, 431, 498 and 488, respectively. In MS^3 step, the former two ions of m/z 429 and 431 lost H_2O, and resulted in ions of m/z 411 and 413, respectively. Both these ions dissociated further in MS^4 step into product ions of m/z 341 and 343 upon common loss of C_4H_6O. In a further step (MS^5), the ion of m/z 341 was fragmented to product ions of m/z 323 (loss of H_2O) and 297 (loss of CO_2), while the ion of m/z 343 formed product ions of m/z 325 and 299, again on losses of H_2O and CO_2, respectively.

The fragment ion of m/z 498, which was formed in MS^2 step, dissociated into product ion of m/z 400 upon loss of H_3PO_4, while another MS^2 step fragment of m/z 488 resulted into ions of m/z 418 (loss of C_4H_6O) and 234 (loss of $C_{12}H_{18}N_2O_2S$), which further dissociated to m/z 190 (loss of C_2H_4O). The product ion of m/z 418, arising from m/z 488, further fragmented into ions of m/z 400, 374, 362, 263 and 261 upon loss of H_2O, CO_2, C_4H_8, $C_6H_5NO_2S$ and $C_6H_7NO_2S$, respectively. The fragment ion of m/z 400, which was common in case of MS^2 precursor ions of m/z 498 and 488, lost $C_6H_7NO_2S$, $C_6H_5NO_2S$, SO_2, C_4H_8 and HCNO to yield product ions of m/z 243, 245, 336, 344 and 357, respectively. The ion of m/z 374 dissociated further into four product ions of m/z 357, 318, 219 and 217 upon neutral loss of NH_3, C_4H_8, $C_6H_5NO_2S$ and $C_6H_7NO_2S$, respectively, while another fragment ion of m/z 362 was converted to a fragment of m/z 318 upon loss of CO_2. The precursor of m/z 263 underwent fragmentation into product ions of m/z 219 (loss of CO_2) and 245 (loss of H_2O). The same losses also occurred in case of m/z 261 leading to ions of m/z 217 and 243. The product ion of m/z 357, which was formed from precursors of m/z 400 and 374, underwent fragmentation into product ions of m/z 301, 293, 255, 253, 202 and 200 upon loss of C_4H_8, SO_2, C_8H_6, C_8H_8, $C_6H_5NO_2S$ and $C_6H_7NO_2S$, respectively. The fragment ion of m/z 344 underwent dissociation to m/z 301 upon loss of HCNO. The product ion of m/z 318, which was formed from the precursors of m/z 374 and 362, lost NH_3 to result in m/z 301. The latter further resulted in ions of m/z 225 (loss of C_6H_4), 173 (loss of $C_{10}H_8$), 156 (loss of $C_{10}H_{11}N$) and 146 (loss of $C_6H_5NO_2S$). No further fragmentation of the product ions of m/z 336, 293 and 253 were observed due to their low abundance. The product ion of m/z 255 underwent fragmentation into m/z 229 (loss of C_2H_2) and 241 (loss of CH_2). Both the ions were further dissociated into a common ion of m/z 156, which further resulted into an ion of m/z 108 by loss of SO. The common ion of m/z 202, which was formed from three different precursor ions of m/z 357, 245 and 219, lost C_4H_8 to yield ion of m/z 146. The latter was also formed from m/z 189 on loss of HCNO and it further dissociated on loss of NH_3 to ion of m/z 129, which was also formed from m/z 172, and was originated on loss of NH_3 from m/z 189. Similarly, ion of m/z 200, which was formed from m/z 357, 243 and 217 on loss of $C_6H_7NO_2S$, HCNO and NH_3, respectively, further dissociated into product ion of m/z 144. Eventually, the product ion of m/z 120 was generated on loss of $C_6H_{13}N$ and $C_6H_{11}N$ from two precursors of m/z 219 and 217, respectively. The whole fragmentation pattern showed unusual losses of SO_2 (m/z 400 → 336 and m/z 357 → 293) and SO (m/z 156 → 108). Such unusual losses are reported during mass fragmentation of sulphonamides [37,38].

3.3. NMR studies on the drug

^1H, ^{13}C, DEPT-135, COSY, TOCSY, HSQC and HMBC NMR spectra of FPV in DMSO-d_6 are shown in Figs. S2–S8 and corresponding data are compiled in Tables 3 and S4. ^1H NMR signals of the drug in DMSO-d_6 included (i) one doublet at δ 6.65 ppm corresponding to aromatic protons H-3 and H-7; (ii) another doublet at δ 7.44 ppm corresponding to the aromatic protons H-4 and H-6; (iii) cluster of multiplets emerging from δ 7.13 to δ 7.25 ppm, corresponding to aromatic protons H-18, H-19, and H-20; (iv) a pair of doublets originating at δ 7.20 ppm corresponding to aromatic methine protons H-17 and H-21; (v) four pairs of multiplets originating at δ 1.91 ppm, δ 4.37 ppm, δ 4.12 ppm, and δ 4.87 ppm corresponding to methine protons H-9, H-13, H-14 and H-24, respectively; (vi) two pairs of doublets arising at δ 0.79 ppm and δ 0.72 ppm corresponding to methyl protons H-10 and H-11, respectively; (vii) five pairs of multiplets corresponding to non-equivalent methylene

Table 2
Interpretation of mass fragmentation data obtained for fosamprenavir (FPV).

Peak No.	Accurate/nominal mass of the observed ion*	Best possible molecular formula	Exact mass of the most probable structure	Error (mmu)	RDB	Possible parent fragment	Mass difference from parent ion	Possible molecular formula for the loss
$[M+H]^+$	586.1963	$C_{25}H_{37}N_3O_9PS^+$	586.1983	−2.0	9.5	–	–	–
a	498.1435	$C_{21}H_{29}N_3O_7PS^+$	498.1458	−2.3	9.5	$[M+H]^+$	88.0525	$C_4H_8O_2$
b	488*	$C_{25}H_{34}N_3O_5S^+$	488.2214	–	10.5	$[M+H]^+$	97.9769	H_3PO_4
c	431*	$C_{19}H_{32}N_2O_7P^+$	431.1942	–	5.5	$[M+H]^+$	155.0041	$C_6H_5NO_2S$
d	429*	$C_{19}H_{30}N_2O_7P^+$	429.1785	–	6.5	$[M+H]^+$	157.0197	$C_6H_7NO_2S$
e	418.1789	$C_{21}H_{28}N_3O_4S^+$	418.1795	−0.6	9.5	b	70.0419	C_4H_6O
f	413*	$C_{19}H_{30}N_2O_6P^+$	413.1836	–	6.5	c	18.0106	H_2O
g	411*	$C_{19}H_{28}N_2O_6P^+$	411.1679	–	7.5	d	18.0106	H_2O
h	400.1680	$C_{21}H_{26}N_3O_3S^+$	400.1689	−0.9	10.5	a	97.9769	H_3PO_4
						e	18.0106	H_2O
i	374.1896	$C_{20}H_{28}N_3O_2S^+$	374.1897	0.0	8.5	e	43.9898	CO_2
j	362.1177	$C_{17}H_{20}N_3O_4S^+$	362.1169	0.8	9.5	e	56.0626	C_4H_8
k	357.1628	$C_{20}H_{25}N_2O_2S^+$	357.1631	−0.3	9.5	h	43.0058	HCNO
						i	17.0265	NH_3
l	344*	$C_{17}H_{18}N_3O_3S^+$	344.1063	–	10.5	h	56.0626	C_4H_8
m	343*	$C_{15}H_{24}N_2O_5P^+$	343.1417	–	5.5	f	70.0419	C_4H_6O
n	341*	$C_{15}H_{22}N_2O_5P^+$	341.1261	–	6.5	g	70.0419	C_4H_6O
o	336*	$C_{21}H_{26}N_3O^+$	336.2070	–	10.5	h	63.9619	SO_2
p	325.1306	$C_{15}H_{22}N_2O_4P^+$	325.1312	−0.6	6.5	m	18.0106	H_2O
q	323*	$C_{15}H_{20}N_2O_4P^+$	323.1155	–	7.5	n	18.0106	H_2O
r	318*	$C_{16}H_{20}N_3O_2S^+$	318.1271	–	8.5	i	56.0626	C_4H_8
						j	43.9898	CO_2
s	301*	$C_{16}H_{17}N_2O_2S^+$	301.1005	–	9.5	k	56.0626	C_4H_8
						l	43.0058	HCNO
						r	17.0265	NH_3
t	299*	$C_{14}H_{24}N_2O_3P^+$	299.1519	–	4.5	m	43.9898	CO_2
u	297*	$C_{14}H_{22}N_2O_3P^+$	297.1363	–	5.5	n	43.9898	CO_2
v	293*	$C_{20}H_{25}N_2^+$	293.2012	–	9.5	k	63.9619	SO_2
w	263.1762	$C_{15}H_{23}N_2O_2^+$	263.1754	0.8	5.5	e	155.0041	$C_6H_5NO_2S$
x	261.1595	$C_{15}H_{21}N_2O_2^+$	261.1598	−0.3	6.5	e	157.0197	$C_6H_7NO_2S$
y	255.1155	$C_{12}H_{19}N_2O_2S^+$	255.1162	−0.7	4.5	k	102.0470	C_8H_6
z	253*	$C_{12}H_{17}N_2O_2S^+$	253.1005	–	5.5	k	104.0626	C_8H_8
aa	245.1645	$C_{15}H_{21}N_2O^+$	245.1648	−0.3	6.5	h	155.0041	$C_6H_5NO_2S$
						w	18.0106	H_2O
bb	243*	$C_{15}H_{19}N_2O^+$	243.1492	–	7.5	h	157.0197	$C_6H_7NO_2S$
						x	18.0106	H_2O
cc	241.1002	$C_{11}H_{17}N_2O_2S^+$	241.1005	−0.3	4.5	y	14.0157	CH_2
dd	234.1123	$C_{13}H_{16}NO_3^+$	234.1125	−0.2	6.5	b	254.1089	$C_{12}H_{18}N_2O_2S$
ee	229.0991	$C_{10}H_{17}N_2O_2S^+$	229.1005	−1.4	3.5	y	26.0157	C_2H_2
ff	225*	$C_{10}H_{13}N_2O_2S^+$	225.0692	–	5.5	s	76.0313	C_6H_4
gg	219*	$C_{14}H_{23}N_2^+$	219.1856	–	4.5	i	155.0041	$C_6H_5NO_2S$
						w	43.9898	CO_2
hh	217*	$C_{14}H_{21}N_2^+$	217.1699	–	5.5	i	157.0197	$C_6H_7NO_2S$
						x	43.9898	CO_2
ii	202.1589	$C_{14}H_{20}N^+$	202.1590	−0.1	5.5	k	155.0041	$C_6H_5NO_2S$
						aa	43.0058	HCNO
						gg	17.0265	NH_3
jj	200.1432	$C_{14}H_{18}N^+$	200.1434	−0.1	6.5	k	157.0197	$C_6H_7NO_2S$
						bb	43.0058	HCNO
						hh	17.0265	NH_3
kk	190.0862	$C_{11}H_{12}NO_2^+$	190.0863	−0.1	6.5	dd	44.0262	C_2H_4O
ll	189.1022	$C_{11}H_{13}N_2O^+$	189.1022	0.0	6.5	aa	56.0626	C_4H_8
mm	173*	$C_6H_9N_2O_2S^+$	173.0379	–	3.5	s	128.0626	$C_{10}H_8$
nn	172*	$C_{11}H_{10}NO^+$	172.0757	–	7.5	ll	17.0265	NH_3
oo	156.0112	$C_6H_6NO_2S^+$	156.0114	−0.2	4.5	s	145.0891	$C_{10}H_{11}N$
						cc	85.0891	$C_5H_{11}N$
						ee	73.0891	$C_4H_{11}N$
pp	146.0963	$C_{10}H_{12}N^+$	146.0964	−0.1	5.5	s	155.0041	$C_6H_5NO_2S$
						ii	56.0626	C_4H_8
						ll	43.0058	HCNO
qq	144*	$C_{10}H_{10}N^+$	144.0808	–	6.5	jj	56.0626	C_4H_8
rr	129.0697	$C_{10}H_9^+$	129.0699	−0.2	6.5	nn	43.0058	HCNO
						pp	17.0265	NH_3
ss	120.0808	$C_8H_{10}N^+$	120.0808	0.0	4.5	gg	99.1048	$C_6H_{13}N$
						hh	97.0891	$C_6H_{11}N$
tt	108.0443	$C_6H_6NO^+$	108.0444	−0.1	4.5	oo	47.9670	SO

* Ions with nominal mass were only observed in MS^n studies.

protons H-8a,b (δ 2.52–2.54 ppm and δ 2.90–2.94 ppm), H-12a,b (δ 2.76–2.80 ppm and δ 3.52–3.54 ppm), H-15a,b (δ 2.55–2.58 ppm and δ 3.00–3.03 ppm), H-25a,b (δ 1.74–1.79 ppm and δ 1.95–1.99 ppm), H-26a,b (δ 3.25–3.28 ppm and δ 3.52–3.54 ppm); (viii) a pair of non-equivalent methylene protons H-27a,b (δ 3.56–3.68 ppm) that co-merged with the moisture signal of DMSO-d_6; and ix) a doublet at δ

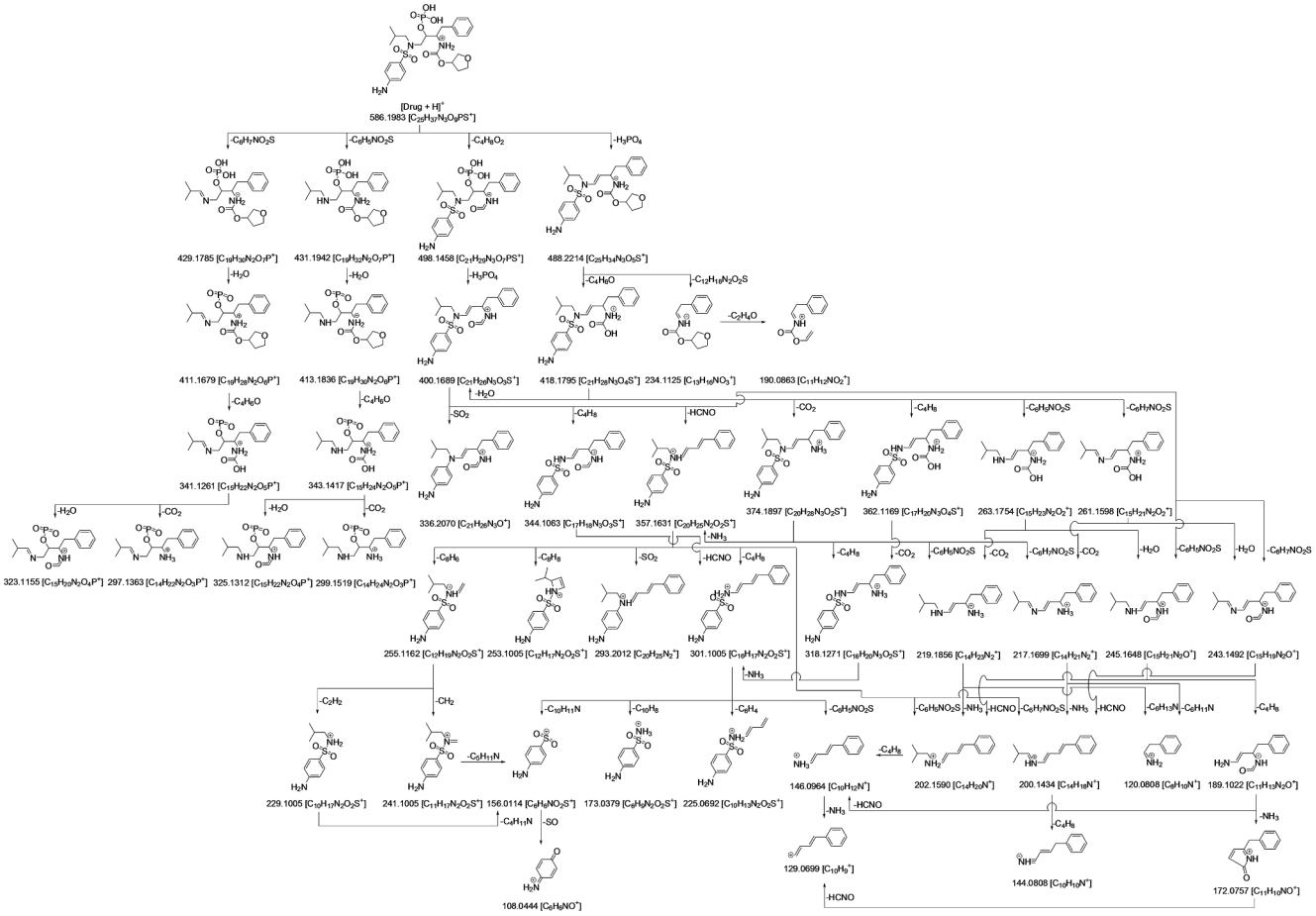

Fig. 2. Mass fragmentation pathway of fosamprenavir (FPV) under ESI positive mode. Values of exact mass and chemical formulae (in square brackets) are given below each structure.

6.89 ppm corresponding to amine proton (carbamate group) H-22.

^{13}C NMR spectrum of the drug (Fig. S3) showed a total of twenty five carbons in the structure. One signal arose at δ 155.70 ppm corresponding to carbonyl at position C-23; aromatic carbon signals at C-2 to C-7 appeared at δ 153.54 ppm, δ 113.34 ppm, δ 129.99 ppm, δ 123.30 ppm, δ 129.99 ppm and δ 113.34 ppm, respectively; aromatic carbon signals for positions C-16 to C-21 appeared at δ 139.54 ppm, δ 129.74 ppm, δ 128.31 ppm, δ 126.33 ppm, δ 128.31 ppm and δ 129.74 ppm, respectively; six signals at δ 58.64 ppm, δ 51.65 ppm, δ 33.77 ppm, δ 32.55 ppm, δ 73.05 ppm and δ 66.68 ppm corresponded to methylene carbons of positions C-8, C-12, C-15, C-25, C-26 and C-27, respectively; two signals at δ 20.55 ppm and δ 20.78 ppm corresponded to methyl carbons at positions C-10 and C-11, respectively; and finally four signals at δ 27.15 ppm, δ 77.24 ppm, δ 53.25 ppm and δ 74.74 ppm corresponded to the methine carbons of positions C-9, C-13, C-14 and C-24, respectively. The position of methyl (C-10 and C-11), methylene (C-8, C-12, C-15, C-25, C-26 and C-27) and methine (C-3, C-4, C-6, C-7, C-9, C-13, C-14, C17-21 and C-24) carbons were differentiated based on DEPT-135 measurement (Fig. S4). Further, HSQC and HMBC studies were carried out to assign connectivities between carbons and protons.

3.4. LC-NMR studies on the drug

Fig. S9 shows peak assignments and multiplicity, based on COSY connectivities in the LC-^{1}H NMR spectrum of the drug. The prominent signals included: (i) one doublet at δ 6.77 ppm corresponding to aromatic protons H-3 and H-7; (ii) another doublet at δ 7.58 ppm corresponding to the aromatic protons H-4 and H-6; (iii) cluster of multiplets emerging from δ 7.22 to δ 7.36 ppm, corresponding to aromatic protons H-17 to H-21; (iv) four pairs of multiplets originating at δ 1.29 ppm, δ 4.77 ppm, δ 4.24 ppm and δ 4.94 ppm corresponding to methine protons H-9, H-13, H-14 and H-24, respectively; (v) two pairs of doublets arising at δ 0.87 ppm and δ 0.82 ppm corresponding to methyl protons H-10 and H-11, respectively, and (vi) five pairs of multiplets corresponding to non-equivalent methylene protons H-8a,b (δ 2.69–2.73 ppm and δ 2.92–2.94 ppm), H-12a,b (δ 2.97–2.99 ppm and δ 3.48–3.52 ppm), H-15a,b (δ 2.62–2.66 ppm and δ 3.12–3.16 ppm), H-25a,b (δ 1.17–1.19 ppm and δ 1.75–1.79 ppm), H-26a,b (δ 2.99–3.04 ppm and δ 3.41–3.43 ppm) and H-27a,b (δ 3.60–3.64 ppm and δ 4.35–4.40 ppm).

3.5. Characterization of the degradation products (DP 1 to DP 6) based on LC-HRMS, LC-MS^{n}, LC-NMR and NMR data

The DPs 1–6 were characterized systematically based on the results of LC-HRMS, LC-MS^{n}, LC-NMR and NMR studies. LC-HRMS line spectra of all the six are shown in Figs. S10–S15. The accurate and exact mass values of the protonated molecule and the fragment ions, along with their molecular formulae, errors (mmu) and RDB, are listed in Table 4. The corresponding LC-MS^{n} data of DPs are listed in Table S5. Overlaid LC-^{1}H NMR spectra of FPV and DP 3 are shown in Fig. 3. 1D and 2D NMR data were obtained for five DPs, which are compiled in Tables 3 and S4, respectively. The coalesced information from various techniques was used for structural elucidation of all the DPs, as discussed below individually.

3.5.1. DP 1 (m/z 392)

The observed accurate mass of DP 1 (Fig. S10, Table 4) was found to be 392.1997 Da, which was 194 Da less than the drug. The nitrogen rule

Table 3
^{1}H, ^{13}C and DEPT-135 data of fosamprenavir (FPV), DP 1, DP 2 and DPs 4–6 in DMSO-d_6.

Chemical structure	FPV 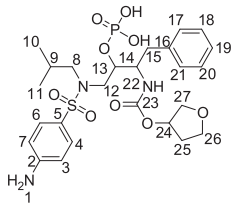			DP 1 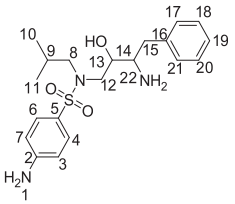			DP 2 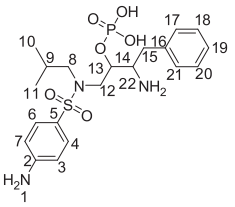		
Position	^{1}H (δ ppm)	^{13}C (δ ppm)	DEPT-135	^{1}H (δ ppm)	^{13}C (δ ppm)	DEPT-135	^{1}H (δ ppm)	^{13}C (δ ppm)	DEPT-135
1	*	–	–	*	–		*	–	–
1′	–	–	–	–	–	–	–	–	–
2	–	153.54	–	–	153.42	–	–	153.55	–
3	6.65 (d)	113.34	CH	6.55 (d)	113.25	CH	6.56 (d)	113.28	CH
4	7.44 (d)	129.99	CH	7.30 (m)	129.92	CH	7.40 (d)	130.14	CH
5	–	123.30	–	–	123.49	–	–	123.35	–
6	7.44 (d)	129.99	CH	7.30 (m)	129.92	CH	7.40 (d)	130.14	CH
7	6.65 (d)	113.34	CH	6.55 (d)	113.25	CH	6.56 (d)	113.28	CH
8a,b	2.52–2.54 (m), 2.90–2.94 (m)	58.64	CH_2	2.50–2.55 (m), 2.74–2.79 (m)	58.00	CH_2	2.51–2.55 (m), 2.85–2.91 (m)	57.85	CH_2
9	1.91 (m)	27.15	CH	1.81 (m)	27.10	CH	1.88 (m)	26.70	CH
10	0.79 (d)	20.55	CH_3	0.74 (d)	20.55	CH_3	0.74 (d)	20.67	CH_3
11	0.72 (d)	20.78	CH_3	0.68 (d)	20.55	CH_3	0.63 (d)	20.67	CH_3
12a,b	2.76–2.80 (m), 3.52–3.54 (m)	51.65	CH_2	2.62–2.67 (m), 3.18–3.22 (m)	52.37	CH_2	2.66–2.70 (m), 3.39–3.44 (m)	51.15	CH_2
13	4.37 (m)	77.24	CH	3.92 (m)	69.86	CH	4.39 (m)	72.49	CH
14	4. 12 (m)	53.25	CH	3.35 (m)	55.58	CH	3.57 (m)	53.64	CH
15a,b	2.55–2.58 (m), 3.00–3.03 (m)	33.77	CH_2	2.69–2.72 (m), 2.94–2.96 (m)	33.58	CH_2	2.66–2.70 (m), 3.14–3.17 (m)	32.79	CH_2
16	–	139.54	–	–	137.91	–	–	137.74	–
17	7.20 (d)	129.74	CH	7.28 (d)	129.56	CH	7.27 (d)	129.61	CH
18	7.25 (m)	128.31	CH	7.28 (m)	129.04	CH	7.34 (m)	129.02	CH
19	7.13 (m)	126.33	CH	7.20 (m)	127.14	CH	7.20 (m)	127.16	CH
20	7.25 (m)	128.31	CH	7.28(m)	129.04	CH	7.34 (m)	129.02	CH
21	7.20 (d)	129.74	CH	7.28 (d)	129.56	CH	7.27 (d)	129.61	CH
22	6.89 (d)	–	–	*	–	–	*	–	–
23	–	155.70	–	–	–	–	–	–	–
24	4.87 (m)	74.74	CH	–	–	–	–	–	–
25a,b	1.74–1.79 (m), 1.95–1.99 (m)	32.55	CH_2	–	–	–	–	–	–
26a,b	3.25–3.28 (m), 3.52–3.54 (m)#	73.05	CH_2	–	–	–	–	–	–
27a,b	3.56–3.68 (m)#	66.68	CH_2	–	–	–	–	–	–

(*continued on next page*)

Table 3 (*continued*)

Chemical structure	DP 4 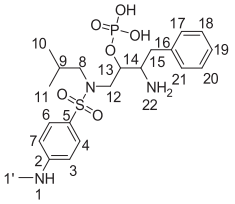			DP 5 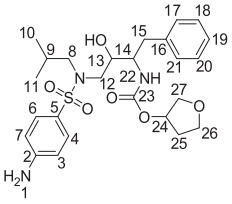			DP 6 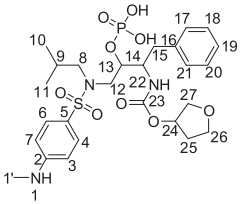		
Position	^{1}H (δ ppm)	^{13}C (δ ppm)	DEPT-135	^{1}H (δ ppm)	^{13}C (δ ppm)	DEPT-135	^{1}H (δ ppm)	^{13}C (δ ppm)	DEPT-135
1	6.61 (m)	–	–	*	–	–	6.60 (m)	–	–
1′	2.68 (d)	29.66	CH_3	–	–	–	2.68 (s)	29.66	CH_3
2	–	153.66	–	–	153.26	–	–	153.66	–
3	6.56 (d)	111.17	CH	6.56 (d)	113.16	CH	6.59 (d)	111.27	CH
4	7.43 (d)	130.08	CH	7.34 (d)	129.66	CH	7.47 (d)	130.15	CH
5	–	123.25	–	–	123.99	–	–	123.07	–
6	7.43 (d)	130.08	CH	7.34 (d)	129.66	CH	7.47(d)	130.15	CH
7	6.56 (d)	111.17	CH	6.56 (d)	113.16	CH	6.59 (d)	111.27	CH
8a,b	2.53–2.57 (m), 2.87–2.90 (m)	57.87	CH_2	2.57–2.59 (m), 2.84–2.89 (m)	57.65	CH_2	2.43–2.45 (m), 2.88–2.92 (m)	58.88	CH_2
9	0.87 (m)	26.73	CH	1.89 (m)	26.90	CH	1.88 (m)	27.32	CH
10	0.77 (d)	20.71	CH_3	0.80 (d)	20.58	CH_3	0.77 (d)	20.55	CH_3
11	0.66 (d)	20.71	CH_3	0.74 (d)	20.58	CH_3	0.72 (d)	20.78	CH_3
12a,b	2.60–2.63 (m), 3.38–3.43 (m)	51.34	CH_2	2.61–2.65 (m), 3.21–3.25 (m)	53.20	CH_2	2.57–2.61 (m), 3.43–3.46 (m)	52.41	CH_2
13	4.37 (m)	72.81	CH	4.88 (m)	74.62	CH	4.18 (m)	75.76	CH
14	3.54 (m)	53.63	CH	3.54 (m)	56.13	CH	4.18 (m)	52.99	CH
15a,b	2.64–2.67 (m), 3.12–3.16 (m)	33.16	CH_2	2.43–2.44 (m)#, 2.95–2.98 (m)	35.62	CH_2	2.46–2.48 (m)#, 2.94–2.98 (m)	34.08	CH_2
16	–	137.95	–	–	140.09	–	–	140.04	–
17	7.32 (m)	129.57	CH	7.17 (m)	129.53	CH	7.17 (d)	129.60	CH
18	7.32 (m)	129.06	CH	7.20 (m)	128.42	CH	7.23 (m)	128.13	CH
19	7.23 (m)	127.18	CH	7.12 (m)	126.26	CH	7.09 (m)	126.07	CH
20	7.32 (m)	129.06	CH	7.20 (m)	128.42	CH	7.23 (m)	128.13	CH
21	7.32 (m)	129.57	CH	7.17 (m)	129.53	CH	7.17 (d)	129.60	CH
22	*	–	–	7.11 (m)	–	–	7.43 (d)	–	–
23	–	–	–	–	156.09	–	–	155.53	–
24	–	–	–	3.57 (m)	72.92	CH	4.78 (m)	74.44	CH
25a,b	–	–	–	1.71–1.76 (m), 1.98–2.05 (m)	32.73	CH_2	1.71–1.76 (m), 1.91–1.97 (m)	32.43	CH_2
26a,b	–	–	–	3.29–3.31 (m), 3.60–3.64 (m)	73.10	CH_2	3.18–3.20 (m), 3.48–3.51 (m)	73.16	CH_2
27a,b	–	–	–	3.46–3.51 (m), 3.66–3.70 (m)	66.68	CH_2	3.53–3.58 (m), 3.65–3.70 (m)	66.69	CH_2

* Signals were not observed, #Signals merge with the moisture peak. Key: s, singlet; d, doublet; m, multiplet.

Table 4
LC-HRMS data of degradation products DPs 1–6 along with their molecular formulae and major fragments in ESI positive mode.

	Accurate mass	Molecular formula	Exact mass	Error (mmu)	RDB	Nitrogen rule	Accurate masses of fragment ions
[DP 1+H]$^+$	392.1997	$C_{20}H_{30}N_3O_3S^+$	392.2002	−0.5	7.5	Odd	375.1726, 374.1886, 357.1631, 336.1371, 319.1088, 318.1260, 301.1024, 271.1108, 255.1166, 241.1003, 237.1963, 235.1793, 229.1003, 220.1691, 219.1853, 218.1536, 217.1698, 202.1589, 200.1434, 164.1070, 156.0112, 146.0965, 129.0698, 120.0808, 108.0448
[DP 2+H]$^+$	472.1662	$C_{20}H_{31}N_3O_6PS^+$	472.1666	−0.4	7.5	Odd	374.1893, 357.1630, 255.1147, 241.1003, 217.1697, 202.1589, 200.1433, 156.0112, 146.0964, 129.0699, 120.0809, 108.0445
[DP 3+H]$^+$	530.1712	$C_{22}H_{33}N_3O_8PS^+$	530.1720	−0.8	8.5	Odd	498.1481, 432.1946, 400.1683, 357.1624, 293.1996, 277.1901, 276.1828, 275.1747, 255.1157, 253.0999, 245.1647, 243.1487, 241.1002, 229.1002, 204.1018, 202.1588, 200.1434, 185.1286, 178.0861, 171.1127, 156.0112, 146.0602, 144.0811, 129.0701
[DP 4+H]$^+$	486.1822	$C_{21}H_{33}N_3O_6PS^+$	486.1822	0.0	7.5	Odd	388.2050, 371.1785, 269.1320, 255.1160, 217.1698, 202.1588, 200.1435, 170.0270, 146.0965, 122.0602, 120.0810
[DP 5+H]$^+$	506.2311	$C_{25}H_{36}N_3O_6S^+$	506.2319	−0.8	9.5	Odd	436.1898, 418.1787, 392.1994, 374.1891, 362.1165, 357.1625, 351.2273, 349.2110, 333.2166, 318.1275, 293.2007, 278.1382, 263.1749, 261.1594, 255.1156, 245.1645, 241.1003, 234.1122, 229.1002, 219.1853, 217.1698, 208.0966, 202.1589, 200.1432, 189.1020, 156.0112, 146.0964, 144.0804, 129.0697, 120.0808, 108.0445
[DP 6+H]$^+$	600.2091	$C_{26}H_{39}N_3O_9PS^+$	600.2139	−4.8	9.5	Odd	512.1584, 502.2395, 432.1949, 431.1936, 414.1837, 413.1834, 388.2047, 371.1793, 368.2333, 343.1425, 333.2171, 325.1309, 299.1512, 269.1316, 263.1753, 261.1595, 255.1154, 245.1647, 234.1125, 219.1869, 202.1594, 200.1437, 190.0862, 189.1021, 170.0269, 146.0958, 129.0699, 122.0600, 120.0810

and elemental composition calculation suggested $C_{20}H_{30}N_3O_3S^+$ (theoretical mass, 392.2002 Da) as its most probable molecular formula. In the MS^2 step, the product ions formed were of *m/z* 375 (loss of NH_3), 374 (loss of H_2O), 336 (loss of C_4H_8), 271 (loss of $C_8H_{11}N$), 237 (loss of $C_6H_5NO_2S$) and 235 (loss of $C_6H_7NO_2S$). The characteristic loss of NH_3 and H_2O in MS^2 step itself clearly suggested that the drug underwent hydrolysis by cleavage of phosphate ester and carbamate moieties. The fragmentation pathway of DP 1 is shown in (Fig. S16), which was found to be overall similar to the drug (Fig. 2), except some unique fragment pathways, *viz.*, *m/z* 336 → 318; 271 → 156; 237 → 220 → 202, 164; 235 → 218 → 200. Hence, the structure of DP 1 could be proposed 4-amino-N-((2R,3S)-3-amino-2-hydroxy-4-phenylbutyl)-N-isobutylbenzenesulfonamide. The structure was supported by NMR results, like ^{1}H NMR spectrum (Fig. S17) showed the absence of protons (H-24 to H-27) related to tetrahydrofuran (THF) ring. Remaining all protons positions were same as the drug, except for signals H-13 (δ 3.92 ppm) and H-14 (δ 3.35 ppm). Both protons showed shielding effect compared to the drug, which confirmed that the hydrolysis could take place at two sites, i.e., phosphate ester and carbamate. Only 20 carbon signals were observed in ^{13}C NMR spectrum (Fig. S18). Absence of signals for C-23 to C-27 suggested the cleavage of C—N bond of carbamate group and absence of THF ring. The same was justified through DEPT-135 (Fig. S19) data. The proton-proton correlations (COSY (Fig. S20) and TOCSY (Fig. S21)) and proton-carbon correlations (HSQC (Fig. S22) and HMBC (Fig. S23)) further supported the proposed structure. 1D and 2D NMR data are provided in Tables 3 and S4, respectively.

3.5.2. DP 2 (m/z 472)

The accurate mass of DP 2 was determined to be 472.1662 Da (Fig. S11), which was 114 Da less than the drug. The RDB, nitrogen rule and elemental composition calculation suggested $C_{20}H_{31}N_3O_6PS^+$ as the best probable molecular formula. The fragmentation pathway of this DP (Fig. S24) was found similar to the drug. This DP had same structure as the drug fragment of *m/z* 374, and followed the same fragmentation scheme, as outlined for the drug in Fig. 2. It highlighted that there was hydrolytic cleavage of carbamate moiety in the drug to yield this DP. The structure was justified by ^{1}H NMR spectrum (Fig. S25), which showed the absence of protons (H-24 to H-27) due to tetrahydrofuran (THF). The decrease in chemical shift of H-14 (δ 3.57 ppm), as compared to the drug, indicated that the change took place adjacent to this hydrogen. In ^{13}C NMR spectrum (Fig. S26), 20 signals were observed, however, none was for the carbonyl group (C-23). DEPT-135 (Fig. S27) data also confirmed the absence of signals for C-24 to C-27. Proton-proton and proton-carbon connectivities for positions C-23 to C-27 were absent in COSY, TOCSY, HSQC and HMBC spectra (Figs. S28–S31). The structure of DP 2 hence could be postulated as (2R,3S)-3-amino-1-(4-amino-N-isobutylphenylsulfonamido)-4-phenylbutan-2-yl dihydrogen phosphate.

3.5.3. DP 3 (m/z 530)

LC-HRMS analysis indicated accurate mass of DP 3 as 530.1712 Da (Fig. S12). Its exact mass was found to be 530.1720 Da (error: −0.8 mmu). Its elemental composition was determined as $C_{22}H_{33}N_3O_8PS^+$. The protonated molecule of DP generated fragment ions of *m/z* 498 (loss of CH_4O) and 432 (loss of H_3PO_4), as depicted in Fig S32. The structure of fragment ion of *m/z* 498 was the same as observed in the drug fragmentation pathway (Fig. 2), where it was generated upon the loss of $C_4H_8O_2$. This suggested the absence of THF moiety. The additional MS^2 fragment of *m/z* 432 was absent in case of the drug. However, a common fragment of *m/z* 400 was found in case of both the drug (Fig. 2) and DP 3 (Fig. S32). In the drug, this ion was formed on loss of water from precursor of *m/z* 418, but the difference in mass in case of DP 3 was 32 Da, which indicated that there was loss of CH_4O. This highlighted that a methyl group substituted THF ring at the same site. The addition of 14 Da was also seen in subsequent fragment ions of *m/z* 277 and 275, which otherwise were of *m/z* 263 and 261, respectively,

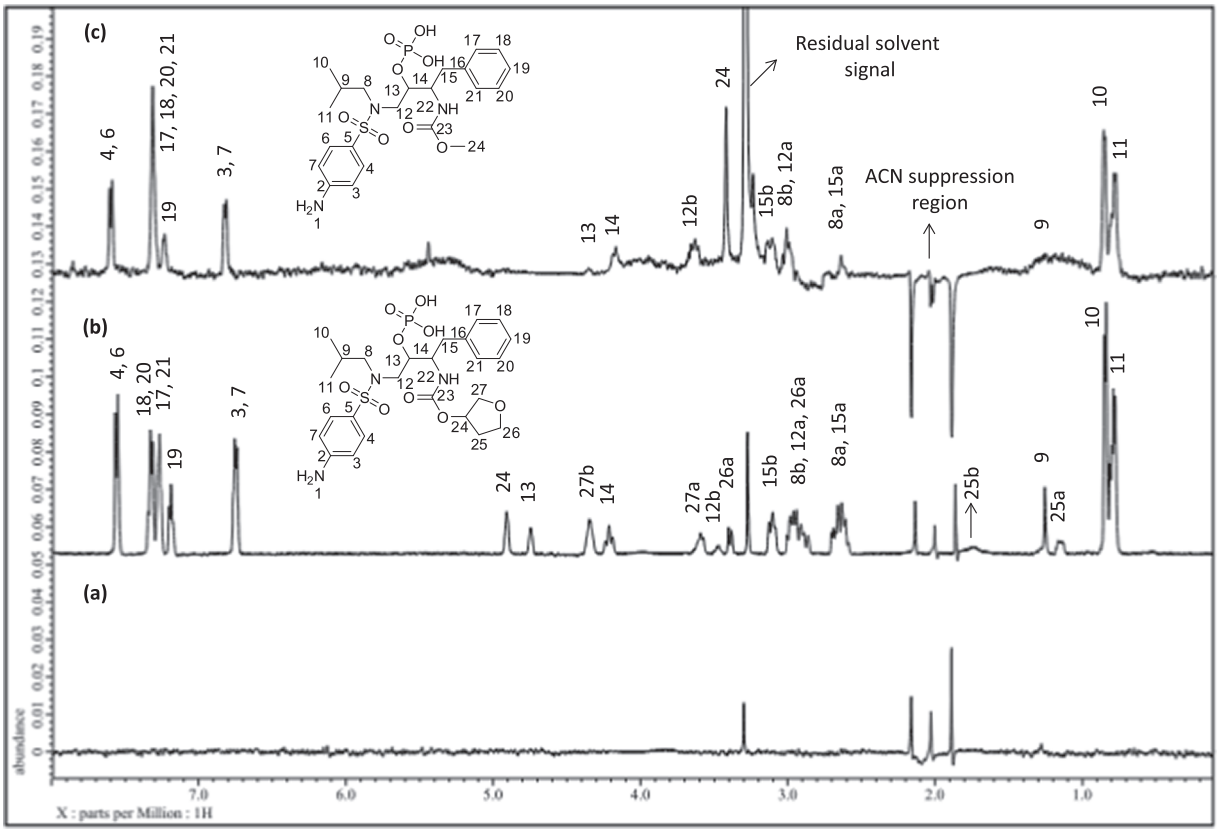

Fig. 3. Overlaid spectrum of LC-^{1}H NMR spectrum of Blank (a), FPV (b) and DP 3 (c).

in the drug. Also the product ions of *m/z* 245 and 243 were generated from precursor ions of *m/z* 277 and 275, respectively upon common loss of CH_4O, whereas the same ions were observed in the case of drug due to the loss of water from the precursors of *m/z* 263 and 261, respectively. These observations clearly supported the structure to be (2R,3S)-3-acetamido-1-(4-amino-N-isobutylphenylsulfonamido)-4-phenylbutan-2-yl dihydrogen phosphate.

This was even confirmed through LC-^{1}H NMR study. Comparative proton NMR data with the drug indicated the absence H-24 to H-27 protons (Fig. 3) of THF moiety, while, an extra signal at δ 3.44 ppm verified the replacement of THF by methyl group at the carbamate moiety.

3.5.4. DP 4 (m/z 486)

The accurate mass of DP 4 was 486.1822 Da (Fig. S13), which was similar to its exact mass. The best probable molecular formula was determined to be $C_{21}H_{33}N_3O_6PS^+$. Its major fragment of *m/z* 388 was generated upon the loss of H_3PO_4, as depicted in Fig. S33. It was 14 Da higher than the drug fragment of *m/z* 374 (Fig. 2). It further dissociated into product ions of *m/z* 371 and 217 on loss of NH_3 and $C_7H_9NO_2S$, respectively. The former yielded product ions of *m/z* 202 and 200 that were structurally similar to those generated in the case of the drug, along with other subsequent fragment ions of *m/z* 146, 144 and 129. There were another product ions of *m/z* 315 and 269 that were 14 Da higher than the drug fragment ions of *m/z* 301 and 255, respectively. The ion of *m/z* 269 further dissociated through the route: *m/z* 269 → 255 (loss of CH_2) → 170 (loss of $C_5H_{11}N$) → 122 (loss of SO). Each of these ions were 14 Da higher than the drug fragment ions of *m/z* 255 → 241 → 156 → 108. Even, the product ions of *m/z* 217, 200, 144 and 120 had the same mass and hence the structures were similar to those present in case of the drug (Fig. 2). It highlighted that the fragmentation pathway of this DP was entirely similar to the drug, except addition of 14 Da in some of the characteristic fragment ions. This observation clearly suggested the presence of methyl moiety at the nitrogen atom of aniline.

In this case, the following salient observations were made from NMR data as compared to the drug:

i. In ^{1}H NMR spectrum (Fig. S34), the absence of H-24 to H-27 protons and decrease in chemical shift value of H-14 (δ 3.54 ppm), as compared to the drug (Fig. S2), confirmed the lack of THF ring. One additional signal was found at δ 2.68 ppm (Table 3), which appeared as doublet for CH_3 attached to the aniline moiety. In COSY and TOCSY studies (Figs. S35 and S36), correlations were observed between H-1′ (δ 2.68 ppm) and H-1 (δ 6.61 ppm). It clearly indicated that methylation occurred at nitrogen of aniline.
ii. The same was further supported by DEPT-135 study (Fig. S37), where one methine (C-24) and three methylene signals (C-25, C-26 and C-27) were not observed. However, one extra signal (C-1′) was observed at δ 29.66 ppm that also established the presence of N-methyl moiety at aniline.
iii. HSQC NMR spectrum (Fig S38) also affirmed the above suggested change.

As pure DP 4 was obtained in very low quantity on enrichment, therefore, HMBC data could not be acquired. From the available results, the structure of this DP could be proposed as (2R,3S)-3-amino-1-(N-isobutyl-4-(methylamino)phenylsulfonamido)-4-phenylbutan-2-yl dihydrogen phosphate.

3.5.5. DP 5 (m/z 506)

The accurate mass of DP 5 (506.2311 Da, Fig. S14) was 80 Da less than the drug. Its most probable molecular formulae was $C_{25}H_{36}N_3O_6S^+$ (error: −0.8 mmu) and had RDB value of 9.5, similar to the drug. Its exact mass of *m/z* 506.2319 was similar to amprenavir, an active moiety of FPV. Its multiple mass fragment ions (Table 4 and S5) of *m/z* 488, 418, 400, 374,

362, 357, 263, 261, 245, 241, 219, 217, 202, 200, 189, 156, 146, 144, 129, 120 and 108 had same mass and structure as to the ones in case of the drug (Fig. 2). Other than these, there were characteristic fragment ions of *m/z* 506 → 488 (loss of H_2O), *m/z* 506 → 462 → 392 → 374 (loss of C_2H_4O, $C_3H_2O_2$ and H_2O), *m/z* 506 → 436 → 418 (loss of C_4H_6O and H_2O) and *m/z* 506 → 351 → 333 (loss of $C_6H_5NO_2S$ and H_2O), which suggested the presence of hydroxyl instead of phosphate ester moiety in the drug molecule. This was supported by the fact that there was no characteristic loss of H_3PO_4 in whole fragmentation pathway of this DP (Fig. S39), which suggested its structure as (S)-tetrahydrofuran-3-yl (2S,3R)-4-(4-amino-N-isobutylphenylsulfonamido)-3-hydroxy-1-phenylbutan-2-ylcarbamate.

In this case, ^{1}H NMR spectrum (Fig. S40) was similar to the drug, except chemical shift value of H-13, which unexpectedly deshielded from δ 4.37 ppm to δ 4.88 ppm, as apparent in Fig. S40, in comparison to Fig. S2. Other NMR data results ^{13}C, DEPT-135, COSY, TOCSY and HSQC (Figs. S41–45) were analogous to the drug along with connectivities (Tables 3 and S4).

To explain the oddity in deshielding of proton at H-13, the co-crystallized structure of amprenavir was taken from the Protein Data Bank (PDB Code: 3EKV) and subjected to quantum chemical analysis using DFT, as discussed in Experimental (Section 2.10). Although numerous conformers were possible, for the sake of verification, three conformers, *viz.*, C1, C2 and C3, whose energetically optimised 3D structures are given in Fig. S46, were taken for the investigation, while maintaining the stereochemistry at the stereocentres. These three were subjected to simulated NMR studies using GIAO method. The calculated ^{1}H NMR chemical shift values of H-13 in conformers C1, C2 and C3 were δ 4.32 ppm, δ 3.28 ppm and δ 4.49 ppm, respectively (Table S6). This revealed that the native conformer C1 was computed to appear in-between C2 and C3 in the simulated NMR spectrum, with clear indication that C3 could deshield at higher ppm value than C1. It justified the unexpected deshielding observed in experimental study, highlighting that there could be a conformer possible in solution state in this case with deshielding of H-13 to δ 4.88 ppm in comparison to δ 4.37 ppm for the same position in FPV. The hydrogen bond interaction computational studies on C3 and FPV were also carried out and the results are shown in Fig. 4. The purpose here was to understand the reason for deshielding of H-13 in C3. Apparently, the same is explained by intramolecular interaction of sulphonyl group present in the vicinity of H-13, which can give rise to S═O···H13 with bond length of 2.3 Å and bond angle of 122.7° for C—H···O (i.e. C13—H13···O═S). In case of FPV, the rotation of H-13 towards the sulphonyl group tends to be hindered due to the presence of phosphate moiety.

3.5.6. DP 6 (*m/z* 600)

This DP had an accurate mass of 600.2091 Da (Fig. S15), with exact mass being 600.2139 Da (error: −4.8 mmu). The protonated molecule formula worked out as $C_{26}H_{39}N_3O_9PS^+$. This indicated that this DP had 14 mass higher than the drug, justified by similar RDB value and fragmentation pattern as the drug (Fig. 2), except MS^2 fragment ions of *m/z* 512, 502, 486 and some of the subsequent product ions with 14 Da higher mass than the respective fragment ions generated from the drug. The structures of the same are shown in Fig. S47, while structures for the product ions with same mass as in Fig. 2, have been skipped. This indicated towards methylation at the aniline moiety. DP 6 in that manner can be said to related to DP 4, it rather being precursor to origin of the latter, which is evident from Fig. S47, where DP 4 is a product ion formed directly from DP 6 on MS^2 fragmentation. This is further proven by similar route of fragmentation of DP 4 (*m/z* 486), as shown in Fig. S33. Based on the results, DP 6 was characterized as (S)-tetrahydrofuran-3-yl (2S,3R)-4-(N-isobutyl-4-(methylamino)phenylsulfonamido)-1-phenyl-3-(phosphonooxy)butan-2-ylcarbamate.

Further support to the structure was provided by ^{1}H (Fig. S48) and DEPT-135 (Fig. S49) NMR data. All chemical shift assignments were done with the help of proton-proton (COSY and TOCSY) and proton-carbon (HSQC and HMBC) correlations spectra of DP 6 as shown in Figs. S50–S53, while corresponding data are compiled in Table S4. NMR studies highlighted the following characteristic features for DP 6, as compared to the drug:

i. ^{1}H NMR spectrum of this DP resembled with the drug spectrum, except one additional signal (H-1′) at δ 2.68 ppm. This signal gave correlation with H-1 (δ 6.60 ppm) in COSY and TOCSY. Data suggested the possibility of methylation at the aniline moiety.
ii. The presence of N-methyl was confirmed by ^{13}C NMR study. An extra signal was observed at δ 29.65 ppm. The same was confirmed even by DEPT-135 experiment.
iii. In HMBC spectrum (Fig. S53), new correlation was observed between H-1′ and C-2, which affirmed methylation of aniline.

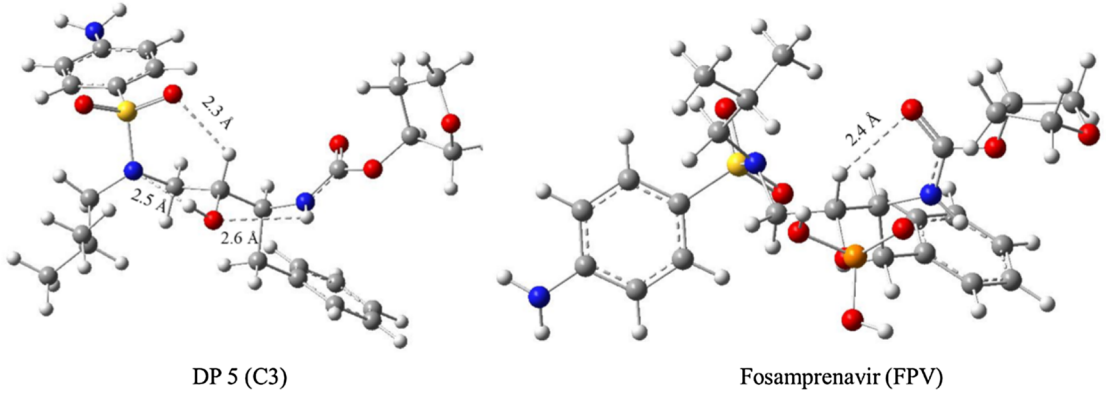

Fig. 4. H-bond interactions of H-13 in DP 5 conformer 3 (C3) and fosamprenavir (FPV).

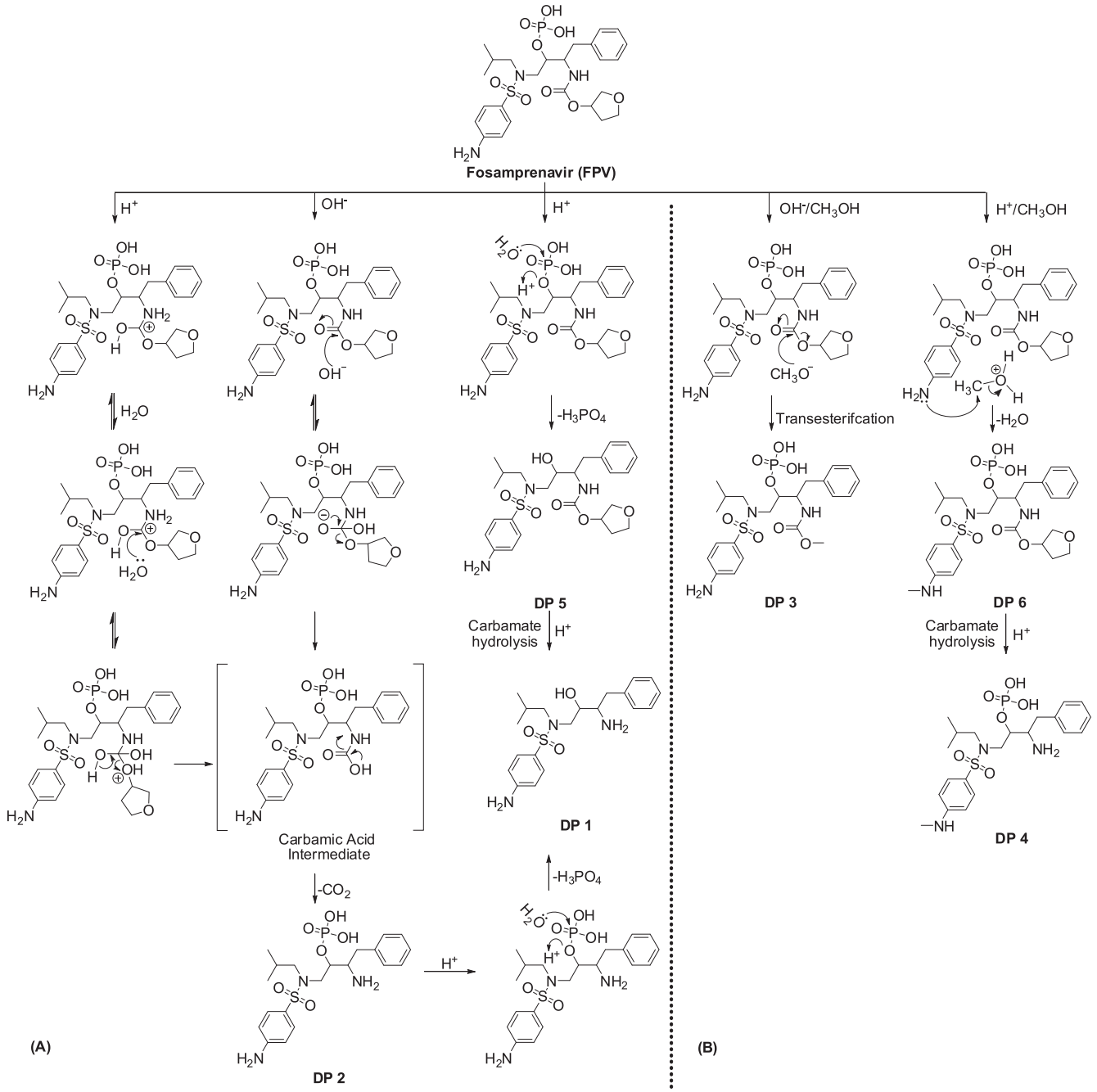

Fig. 5. Degradation pathway and mechanism of hydrolysis of fosamprenavir (FPV). Scheme (A) represents pathway for the formation of real DPs 1, 2 and 5 while scheme (B) suggests pathway for the pseudo DPs 3, 4 and 6.

3.6. Postulated degradation pathway and mechanism of degradation of fosamprenavir

The characterization of DPs 1–6, as discussed above, gave us a clear picture that only DP 1, 2 and 5 were the real DPs of FPV. Other three, *viz.*, DPs 3, 4 and 6 were identified as methylated products, which can be said as pseudo DPs, originating on methylation of the drug due to the presence of methanol, used as a co-solvent for preparing the stress solution. The mechanistic explanation of generation of all the six DPs in different stress solutions is outlined in Fig. 5. Under acidic environment, the drug hydrolysis occurred *via* two routes; (i) hydrolysis of carbamic ester (carbamate) moiety, resulting into the corresponding carbamic acid intermediate, which was unstable in nature and further underwent facile decarboxylation to form DP 2. The latter was further converted into DP 1 through hydrolysis of phosphate ester moiety, and (ii) hydrolysis of phosphate ester moiety, resulting in DP 5. This DP underwent carbamate hydrolysis to form DP 1 in acidic condition. Only DP 2 was a common degradation product formed upon alkaline hydrolysis, which highlighted stability of phosphate ester moiety against hydrolysis in alkali, in comparison to acid.

In the presence of methanol used as a co-solvent, DP 3 could be formed by base-catalyzed trans-esterification reaction. Its mechanistic explanation is that the methoxide ion (a nucleophile), which was formed by removal of proton from methanol in the presence of base, reacted with carbonyl carbon of the drug to give a tetrahedral intermediate, which proceeded further to yield the transesterfied product DP 3. The formation of DP 6 involved N-methylation of drug (at aniline nitrogen) through loss of water, in the presence of acidic methanol. It

further underwent carbamate hydrolysis to result in DP 4.

The pseudo DPs, in some manner, can also be considered important in case of FPV as methanol is used in its synthesis [39,40]. There is propensity for the formation of drug-methanol adduct impurities if methanol is present as a residual solvent in the final drug substance.

3.7. Prediction of physicochemical, and absorption, distribution, metabolism, excretion, and toxicity properties of degradation products and comparison with those of the drug

The in silico predicted ADMET properties of FPV and its DPs are summarized in Table S7. The lipophilicity of DPs 1, 5 and 6 was higher than the drug, while DPs 2–4 were less lipophilic in comparison. The aqueous solubility of the drug and all DPs was predicted to be in the range of 0.172–2.735 mg/mL. Their dissociation constant (pKa), human effective jejunal permeability, apparent Madin-Darby Canine Kidney (MDCK) cells-on-sheet (COS) permeability, permeability through human skin, logarithm of brain/blood partition coefficient (logBB), volume of distribution (Vd, L/kg), blood-to-plasma concentration ratio in human (RBP) and fraction unbound in human liver microsomes values are collated in Table S7. DP 5 was predicted to be substrate for P-glycoprotein (P-gp), while rest of the DPs and the drug were found to be non-substrate as well as non-inhibitor of P-glycoprotein. Similarly, the drug and DPs 3 and 6 were predicted as membrane protein transport (OATP1B1) inhibitors. DPs 1, 5 and 6 were predicted to be CYP2C19 inhibitors. Additionally, DP 5 was predicted to be inhibitor of CYP2C9 and CYP3A4, while DP 1 was found to inhibit only the latter enzyme. The drug and DPs 1, 3, 5 and 6 were predicted to be substrate for CYP3A4. Similarly, the DPs 3 and 4 were found to be substrate for CYP2B6, while DPs 1 and 5 were labile to CYP2C8. Moreover, DP 1 was also found to be substrate for CYP2C9 and CYP2D6. The drug and DPs 1–4 and 6 were found to be negative for reproductive toxicity, while only DP 5 showed the susceptibility. DPs 1 and 5 were predicted as causative for chronic toxicity in rats, while the median toxic dose (TD50) of DPs 1 and 5 in rat was found to be very low, being 5.43 and 4.73 mg/kg/day, respectively, highlighting carcinogenicity in rat. No potential *in silico* mutagenicity was observed for the drug and its DPs. Out of the ten mutagenic models, only MUT_102 + wp2 (*S. typhimurium* strain TA102 and *E. coli* strain WP2 uvrA) showed mutagenic potential for DPs 2 and 4.

4. Conclusion

The present study provided comprehensive degradation chemistry of FPV under acidic and basic stress conditions. A total of six DPs were formed under studied hydrolytic environment. The same were characterized by using LC-HRMS, LC-MS^n, LC-NMR and NMR data. Additionally, i*n silico* physicochemical and ADMET profiles of the drug and its DPs were established, which provided useful insights into their properties. The information provided is expected to be very useful for generic drug manufacturer during product development and monitoring of product quality of this important anti-HIV agent.

Acknowledgement

The authors gratefully acknowledge Simulations Plus (Lancaster, CA, USA) for providing license assess to ADMET Predictor™ (version 9.0.0.10). We are thankful to Prof. A. K. Chakraborti, Department of Medicinal Chemistry, NIPER, S.A.S. Nagar for his valuable scientific suggestions.

Appendix A. Supplementary material

Supplementary data to this article can be found online at https://doi.org/10.1016/j.ejpb.2019.06.018.

References

[1] M. Bakshi, S. Singh, Development of validated stability-indicating assay methods-critical review, J. Pharm. Biomed. Anal. 28 (2002) 1011–1040.
[2] R. Canavesi, S. Aprile, G.B. Giovenzana, A. Di Sotto, S. Di Giacomo, E. Del Grosso, G. Grosa, New insights in oxybutynin chemical stability: identification in transdermal patches of a new impurity arising from oxybutynin N-oxide rearrangement, Eur. J. Pharm. Sci. 84 (2016) 123–131.
[3] B.S. Kushwah, J. Gupta, D.K. Singh, M. Kurmi, A. Sahu, S. Singh, Characterization of solution stress degradation products of aliskiren and prediction of their physicochemical and ADMET properties, Eur. J. Pharm. Sci. 121 (2018) 139–154.
[4] B. Lajin, O. Steiner, L. Fasshold, K. Zangger, W. Goessler, The identification and chromatographic separation of a new highly analogous impurity of the active pharmaceutical ingredient icatibant, Eur. J. Pharm. Sci. 132 (2019) 121–124.
[5] M. Lecoeur, V. Vérones, C. Vaccher, J.-P. Bonte, N. Lebegue, J.-F. Goossens, Structural elucidation of degradation products of a benzopyridooxathiazepine under stress conditions using electrospray orbitrap mass spectrometry – study of degradation kinetic, Eur. J. Pharm. Sci. 45 (2012) 559–569.
[6] D.K. Singh, M. Kurmi, T. Handa, S. Singh, LC-MS/TOF, LC-MS^n and H/D exchange studies on solifenacin succinate targeted to characterize its forced degradation products, Chromatographia 79 (2016) 159–168.
[7] D.K. Singh, A. Sahu, T. Handa, M. Narayanam, S. Singh, Study of the forced degradation behavior of prasugrel hydrochloride by liquid chromatography with mass spectrometry and liquid chromatography with NMR detection and prediction of the toxicity of the characterized degradation products, J. Sep. Sci. 38 (2015) 2995–3005.
[8] S. Singh, T. Handa, M. Narayanam, A. Sahu, M. Junwal, R.P. Shah, A critical review on the use of modern sophisticated hyphenated tools in the characterization of impurities and degradation products, J. Pharm. Biomed. Anal. 69 (2012) 148–173.
[9] E.U. Stolarczyk, A. Rosa, M. Kubiszewski, J. Zagrodzka, M. Cybulski, Ł. Kaczmarek, Use of the hyphenated LC-MS/MS technique and NMR/IR spectroscopy for the identification of exemestane stress degradation products during the drug development, Eur. J. Pharm. Sci. 109 (2017) 389–401.
[10] S.K. Tiwari, D.K. Singh, M.K. Ladumor, A.K. Chakraborti, S. Singh, Study of degradation behaviour of montelukast sodium and its marketed formulation in oxidative and accelerated test conditions and prediction of physicochemical and ADMET properties of its degradation products using ADMET Predictor™, J. Pharm. Biomed. Anal. 158 (2018) 106–118.
[11] T.M. Chapman, G.L. Plosker, C.M. Perry, Fosamprenavir. Drugs 64 (2004) 2101–2124.
[12] M.B. Wire, M.J. Shelton, S. Studenberg, Fosamprenavir, Clin. Pharmacokinet. 45 (2006) 137–168.
[13] C. Baker, P. Chaturvedi, M. Hale, G. Bridson, A. Heiser, E. Furfine, A. Spaltenstein, R. Tung, Discovery of VX-175/GW433908, a novel, water-soluble prodrug of amprenavir, 39th Interscience Conference on Anti-microbial Agents and Chemotherapy, San Francisco, 1999, p. 26–29.
[14] S. Noble, K.L. Goa, Amprenavir. Drugs 60 (2000) 1383–1410.
[15] M. Chilukuri, P. Narayanareddy, K. Hussianreddy, Stability-indicating HPLC method for determination of fosamprenavir calcium, J. Chromatogr. Sci. 52 (2013) 781–787.
[16] S.S. Pekamwar, G.B. Bhavar, K.B. Aher, S.J. Kakad, Development of high performance liquid chromatography (HPLC) method for the estimation of fosamprenavir calcium in pharmaceutical formulation, Austin Chromatogr. 2 (2015) 1035–1041.
[17] N.M. Rao, D. Gowrisankar, Development and validation of stability indicating RP-HPLC method for estimation of fosamprenavir calcium in pure and pharmaceutical dosage forms, Asian J. Chem. 27 (2015) 3484.
[18] M. Kurmi, V.M. Golla, S. Kumar, A. Sahu, S. Singh, Stability behaviour of antiretroviral drugs and their combinations. 1: characterization of tenofovir disoproxil fumarate degradation products by mass spectrometry, RSC Adv. 5 (2015) 96117–96129.
[19] M. Kurmi, B.S. Kushwah, A. Sahu, M. Narayanam, S. Singh, Stability behaviour of antiretroviral drugs and their combinations. 2: characterization of interaction products of lamivudine and tenofovir disoproxil fumarate by mass and NMR spectrometry, J. Pharm. Biomed. Anal. 125 (2016) 245–259.
[20] M. Kurmi, D.K. Singh, S. Tiwari, P. Sharma, S. Singh, Stability behaviour of antiretroviral drugs and their combinations. 3: characterization of interaction products of emtricitabine and tenofovir disoproxil fumarate by mass spectrometry, J. Pharm. Biomed. Anal. 128 (2016) 438–446.
[21] V.M. Golla, M. Kurmi, K. Shaik, S. Singh, Stability behaviour of antiretroviral drugs and their combinations. 4: characterization of degradation products of tenofovir alafenamide fumarate and comparison of its degradation and stability behaviour with tenofovir disoproxil fumarate, J. Pharm. Biomed. Anal. 131 (2016) 146–155.
[22] M. Kurmi, A. Sahu, S. Singh, Stability behaviour of antiretroviral drugs and their combinations. 5: characterization of novel degradation products of abacavir sulfate by mass and nuclear magnetic resonance spectrometry, J. Pharm. Biomed. Anal. 134 (2017) 372–384.
[23] M. Kurmi, A. Sahu, S.K. Tiwari, S. Singh, Stability behaviour of antiretroviral drugs and their combinations. 6: evidence of formation of potentially toxic degradation products of zidovudine under hydrolytic and photolytic conditions, RSC Adv. 7 (2017) 18803–18814.
[24] M. Kurmi, S. Singh, Stability behavior of antiretroviral drugs and their combinations. 7: comparative degradation pathways of lamivudine and emtricitabine and explanation to their differential degradation behavior by density functional theory, J. Pharm. Biomed. Anal. 142 (2017) 155–161.
[25] M. Kurmi, A. Sahu, D.K. Singh, I.P. Singh, S. Singh, Stability behaviour of

antiretroviral drugs and their combinations. 8: characterization and in-silico toxicity prediction of degradation products of efavirenz, J. Pharm. Biomed. Anal. 148 (2018) 170–181.
[26] M. Kurmi, A. Sahu, M.K. Ladumor, A. Kumar Bansal, S. Singh, Stability behaviour of antiretroviral drugs and their combinations. 9: identification of incompatible excipients, J. Pharm. Biomed. Anal. 166 (2019) 174–182.
[27] Guideline, 1996. ICH Q1B. Photostability Testing of New Drug Substances and Products.
[28] S. Singh, M. Junwal, G. Modhe, H. Tiwari, M. Kurmi, N. Parashar, P. Sidduri, Forced degradation studies to assess the stability of drugs and products, Trends Anal. Chem. 49 (2013) 71–88.
[29] S. Singh, M. Bakshi, Guidance on the conduct of stress tests to determine inherent stability of drugs, Pharm. Technol. On-Line (2000) 1–14.
[30] M. Frisch, G. Trucks, H. Schlegel, G. Scuseria, M. Robb, J. Cheeseman, G. Scalmani, V. Barone, B. Mennucci, G. Petersson, Gaussian 09, EM64L-G09RevB. 01. Gaussian Inc, Wallingford CT, 2010.
[31] C. Lee, W. Yang, R.G. Parr, Development of the Colle-Salvetti correlation-energy formula into a functional of the electron density, Phys. Rev. B 37 (1988) 785.
[32] R.G. Parr, Density Functional Theory of Atoms and Molecules, Horiz Quantum Chem, Springer, 1980, pp. 5–15.
[33] G. Schreckenbach, T. Ziegler, Calculation of NMR shielding tensors using gauge-including atomic orbitals and modern density functional theory, J. Phys. Chem. 99 (1995) 606–611.
[34] K. Wolinski, J.F. Hinton, P. Pulay, Efficient implementation of the gauge-independent atomic orbital method for NMR chemical shift calculations, J. Am. Chem. Soc. 112 (1990) 8251–8260.
[35] S.S. Chourasiya, A.A. Wani, C. Nagaraja, A.K. Chakraborti, P.V. Bharatam, N-(acridin-9-yl) arenesulfonamides: synthesis, quantum chemical studies and crystal structure analysis to establish the tautomeric preferences, Tetrahedron 74 (2018) 3634–3641.
[36] https://www.simulations-plus.com/software/admetpredictor/ (accessed 14 March 2019).
[37] M. Sun, W. Dai, D.Q. Liu, Fragmentation of aromatic sulfonamides in electrospray ionization mass spectrometry: elimination of SO_2 via rearrangement, J. Mass Spectrom. 43 (2008) 383–393.
[38] H.Y. Wang, X. Zhang, Y.L. Guo, X.C. Dong, Q.H. Tang, L. Lu, Sulfonamide bond cleavage in benzenesulfonamides and rearrangement of the resulting p-aminophenylsulfonyl cations: application to a 2-pyrimidinyloxybenzylaminobenzenesulfonamide herbicide, Rapid Commun. Mass Spectrom. 19 (2005) 1696–1702.
[39] < https://patentimages.storage.googleapis.com/08/73/6d/f77d4387cf58a0/US9085592.pdf > (accessed 26 March 2019).
[40] < https://patentimages.storage.googleapis.com/60/c5/40/8b5b47e394f2bd/US8877947.pdf > (accessed 26 March 2019).